Stress orientations at intermediate angles to the San Andreas Fault, California

Jeanne L. Hardebeck and Andrew J. Michael
U.S. Geological Survey, Menlo Park, California, USA

Received 17 June 2004; revised 25 August 2004; accepted 1 September 2004; published 9 November 2004.

[1] There are currently two competing models for the frictional strength of the San Andreas Fault in California: the strong-fault model and the weak-fault model. The strong-fault model predicts the maximum horizontal compressive stress axis to be at low angles to the fault, while the relatively weak fault model predicts it to be at high angles. Previous studies have disagreed as to which model is supported by observed stress orientations. We review and compare these studies and present results from several new focal mechanism stress inversions. We find that the observed stress orientations of different studies are generally consistent, implying that the disagreement is one of interpretation. The majority of studies find compressive stress orientations at intermediate angles to the fault, not strictly consistent with either current model. The strong-fault model is acceptable if the San Andreas is assumed to be a nonoptimally orientated fault that fails because optimally oriented, preexisting planes are not present. The relatively weak fault model is not consistent with the stress orientations. We propose two alternative models to better explain the observed intermediate stress orientations: an intermediate-strength San Andreas model and a model in which all major active faults are weak. *INDEX TERMS:* 7209 Seismology: Earthquake dynamics and mechanics; 7230 Seismology: Seismicity and seismotectonics; 8164 Tectonophysics: Stresses—crust and lithosphere; *KEYWORDS:* fault strength, San Andreas Fault, stress

Citation: Hardebeck, J. L., and A. J. Michael (2004), Stress orientations at intermediate angles to the San Andreas Fault, California, *J. Geophys. Res.*, *109*, B11303, doi:10.1029/2004JB003239.

1. Introduction

[2] Fault strength is an important factor in understanding earthquake occurrence. The strength of a fault, and the magnitude and orientation of the stresses acting on it, may control where and when an earthquake nucleates, how the rupture propagates, and how the stress changes due to one earthquake may trigger another. However, fault strength, and how it may vary in space and time, is still poorly understood.

[3] The strength of the San Andreas Fault (SAF) in California (Figure 1), in particular, has been the subject of controversy for decades [e.g., *Brune et al.*, 1969]. It has been proposed that the SAF is an order of magnitude weaker than other faults [*Zoback et al.*, 1987]. The SAF is a major fault with high displacement and may have developed fault zone structure, mineralogy, or pore fluid pressure different from low-displacement faults, resulting in differences in strength and behavior. If this is the case, models of earthquake behavior from studies of other faults may not be directly applicable to the SAF. It is therefore important to resolve whether the SAF is truly significantly weaker than other faults.

[4] Laboratory measurements indicate that faults should have a high frictional strength, with a coefficient of friction, μ, of 0.6–0.85 [e.g., *Byerlee*, 1978]. Measurements in deep boreholes find deviatoric stress ($[\sigma_1 - \sigma_3]/2$, where σ_1 and σ_3 are the maximum and minimum compressive stresses, respectively) on the order of 100 MPa at seismogenic depths [e.g., *Townend and Zoback*, 2000; *Brudy et al.*, 1997]. These observed stresses are consistent with a high-strength crust, containing only strong faults with $\mu = 0.6–0.85$.

[5] Frictional resistance of ~100 MPa during earthquake slip should produce frictional heating, and an observable heat flow anomaly should appear along the fault if the heat is conducted to the surface. However, no such anomaly has been observed along the SAF, constraining $\mu \leq 0.1–0.2$ [e.g., *Brune et al.*, 1969; *Lachenbruch and Sass*, 1992]. It has been proposed that the frictionally generated heat may be laterally transported by fluids [e.g., *Scholz*, 2000; *Scholz and Hanks*, 2004] and hence not observed as an anomaly along the fault. However, modeling of topography-driven fluid flow indicates that this mechanism is inadequate to explain the lack of an observed heat flow anomaly [*Saffer et al.*, 2003]. Geochemical evidence for short-term, near-fault frictional heating is also lacking, constraining $\mu \leq 0.4$ [*d'Alessio et al.*, 2003].

[6] In light of these discrepant observations, arguments have been made for two end-member models of the strength the SAF (Table 1, first two models). The first is the strong-fault model, in which the SAF has static frictional strength equivalent to laboratory values and the lack of observed heat flow anomaly is explained either by fluid transport of

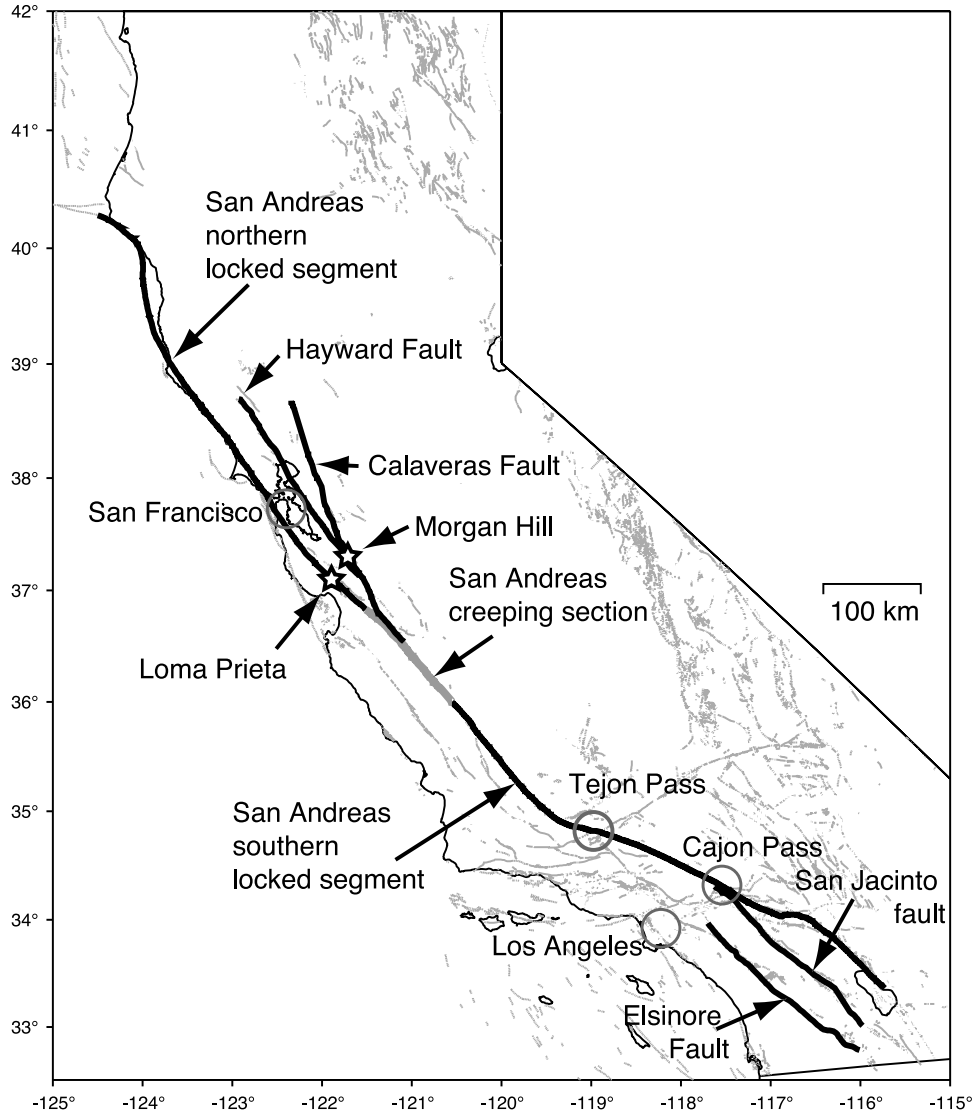

Figure 1. Map of the San Andreas Fault system, California. Mapped surface traces of faults [*Jennings*, 1975] are shown in gray. Major faults of the San Andreas system are shown in black.

heat [e.g., *Scholz*, 2000; *Scholz and Hanks*, 2004] or by dynamic weakening of the fault during rupture [e.g., *Melosh*, 1996; *Andrews and Ben-Zion*, 1997]. The second is the relatively weak fault model, so-called because it requires the SAF to be weak relative both to laboratory samples and to other crustal faults [e.g., *Zoback et al.*, 1987]. In this model, most faults have $\mu = 0.6–0.85$ or frictional strength on the order of 100 MPa, while the SAF is approximately an order of magnitude weaker, with $\mu < 0.1$ or strength on the order of 10 MPa. This low strength may be the result of high pore fluid pressure [e.g., *Rice*, 1992; *Sibson*, 1992] or of the presence of intrinsically weak material in the fault zone.

[7] These two models predict very different stress tensor orientations in the vicinity of the SAF, and hence observed stress orientations should be useful in discriminating be-

Table 1. Three End-Member Models of the Strength of the San Andreas Fault

	High-Stress Crust		Low-Stress Crust
	Strong SAF (Strong-Fault Model[a])	Weak SAF (Relatively Weak Fault Model[a])	Weak SAF (All Faults Are Weak Model)
Stress in surrounding crust, MPa	~100	~100	~10
Typical fault strength, MPa	~100 ($\mu = 0.6$)	~100 ($\mu = 0.6$)	~10 ($\mu < 0.1$)
SAF strength, MPa	~100 ($\mu = 0.6$)	~10 ($\mu < 0.1$)	~10 ($\mu < 0.1$)
The σ_1 angle to SAF	low (30°) to intermediate (60°) angle	high angle (70°–90°)	low to high, depends on the time in the seismic cycle

[a]Prominent in the literature.

Table 2. Compilation of σ_H Orientations Near the SAF Found From the Inversion of Earthquake Focal Mechanisms

Region (Location for Local Study)	Study	σ_H Angle to SAF	Proximity to SAF, km
Northern California	*Provost and Houston* [2003]	50°–55°	≤8
Northern California/Bay Area	this study	50°–60°	≤2
Northern California/Bay Area	this study	∼55°	≤∼10
Bay Area	*Provost and Houston* [2003]	50°–55°	≤8
Bay Area (peninsula near San Jose)	*Townend and Zoback* [2001]	∼84°	≤10
Bay Area (Loma Prieta, premain shock and off-rupture aftershocks)	*Michael et al.* [1990]	∼50°–80°	≤∼10
Bay Area (Loma Prieta, aftershocks, on rupture)	*Michael et al.* [1990]	too heterogeneous	
Bay Area (Loma Prieta, all aftershocks)	*Zoback and Beroza* [1993]	∼77°	≤∼10
Creeping section	*Provost and Houston* [2001]	∼45°	≤∼1–3
Creeping section	*Provost and Houston* [2001]	∼80°	>∼1–3
Southern California	*Jones* [1988]	∼65°	≤10
Southern California	*Hardebeck and Hauksson* [1999]	40°–50°	≤5–20
Southern California	*Townend and Zoback* [2001]	50°–78°	≤∼30
Southern California	this study	40°–50°	≤2
Southern California	this study	∼55°	≤∼10

tween them. If the SAF is as strong as the rest of the crust, it should be optimally oriented for failure, and the maximum horizontal compressive stress axis (σ_H) should be at low angle, ∼30°, to the fault strike. If the SAF is a relatively weak fault in a high-stress crust, it must be oriented such that relatively little shear stress is resolved onto the fault plane. The σ_H axis should then be at high angle, ∼80°, to the fault strike.

[8] Measurements of stress orientation at seismogenic depths have been made along the SAF, primarily from the inversion of earthquake focal mechanisms (Table 2). Some studies report σ_H at high angles to the fault, and some report low angles, leaving it unclear which model is the most consistent with stress observations. The lack of consensus is striking in two recent articles, by *Scholz* [2000] and *Zoback* [2000], which both reviewed the prior work and came to opposite conclusions as to whether stress observations support a strong or a weak SAF.

[9] The purpose of this paper is to investigate the controversy over stress orientation and fault strength, to identify the causes of disagreement, and to propose a solution. If the disagreement comes from discrepancies in the observed stress orientations, this would indicate flawed methodology or focal mechanism data, and the solution would be to rectify the methodology or to improve the focal mechanisms. If, on the other hand, the observed stress orientations prove to be similar, the disagreement must stem from differences in interpretation. In this case, the interpretations must be reevaluated, perhaps in terms of models other than the two major end-members discussed above.

2. Prior Stress Orientation Observations

[10] Early work was generally interpreted as supporting the high-angle, relatively weak fault model. *Zoback et al.* [1987] proposed the relatively weak model for the SAF in central California on the basis of a compilation of borehole stress measurements, geologic features, and focal mechanisms of large earthquakes that implied fault normal compression. *Jones* [1988] inverted the focal mechanisms of small earthquakes along the SAF in southern California and found σ_H orientations 63°–68° to the fault strike along most of the SAF. *Jones* [1988] interpreted these as high angles and hypothesized that the SAF in southern California is weak but not as weak as in central California.

[11] More controversial were the differing interpretations of the aftershock sequence of the 1989 Loma Prieta earthquake in northern California, which contained both left-lateral and right-lateral events on fault planes subparallel to the main shock. *Zoback and Beroza* [1993] claimed that the somewhat different average orientations of the left- and right-lateral events were consistent with slip on low-strength faults under fault normal compression. They inverted the aftershock focal mechanisms for stress and found σ_H oriented 77° to the strike of the SAF, which they interpreted as high angle. *Michael et al.* [1990] and *Michael and Eberhart-Phillips* [2000], however, argued that the high misfit of the focal mechanisms to the best fitting stress tensor implied that the post–Loma Prieta stress field was highly heterogeneous and could not be reliably found by inversion.

[12] Stress orientations inferred from focal mechanisms elsewhere along the SAF in central and northern California produced apparently conflicting results as well. *Townend and Zoback* [2001] concluded that the σ_H orientation in the San Francisco Bay Area is at high angle to the SAF. *Provost and Houston* [2001, 2003] found σ_H along major strike-slip faults of the SAF system oriented at 40°–60° to the fault strike in northern California and the Bay Area. The off-fault σ_H orientation varied along strike from 40°–70° in northern California to 50°–80° in the Bay Area to 70°–90° along the central California creeping section. They interpret their observations in terms of an evolution of fault strength, from a younger, stronger fault in the north to an older, weaker fault in the south.

[13] In southern California, controversy arose over the stress orientation measurements made to ∼3.5 km depth in the Cajon Pass borehole, ∼4 km from the SAF. The observed σ_H orientations [*Zoback and Healy*, 1992] were 63° ± 19° (1σ) to the local fault strike but in a left-lateral sense, whereas the SAF is a right-lateral fault. *Zoback and Healy* [1992] interpreted the lack of right-lateral shear stress on the SAF to mean that the fault is weak. *Scholz and Saucier* [1993], however, presented a model in which the left-lateral orientation is the result of local bends in the fault and the stress orientation at Cajon Pass is insensitive to the magnitude of shear stress on the SAF. If this model is correct, then the Cajon Pass stress orientation measurements contain no information about the strength of the SAF.

[14] There is also debate over stress orientations inferred from focal mechanisms along the SAF in southern California. *Hardebeck and Hauksson* [1999] found that the orientation of σ_H rotated from high angles (60°–100°) in the far field to angles of 40°–50° in a ~10 km wide zone along the SAF, which they interpreted as low angle. Borehole measurements close to the fault also show a rotation, with σ_H at 25°–45° to the strike within ~20 km of the SAF [*Castillo and Hickman*, 2000]. However, *Townend and Zoback* [2001, 2004] inverted the same focal mechanism data set as *Hardebeck and Hauksson* [1999] and found near-fault σ_H orientations with an average orientation of 64°–68° to the SAF, which they interpret as high angle.

3. Stress Orientations in Southern California

3.1. Comparison of Previous Studies

[15] We perform a detailed comparison of two studies that started with the same focal mechanism data set and reached opposite conclusions about the orientation of stress near the SAF in southern California. These studies used the same data, and the same inversion technique for fitting a stress tensor to a set of focal mechanisms, narrowing down the possible sources of discrepancy in the reported results.

[16] *Hardebeck and Hauksson* [1999] and *Townend and Zoback* [2001, 2004] used the same focal mechanism data set for southern California, composed of ~50,000 earthquakes occurring 1981–1999 recorded by the Southern California Seismic Network (SCSN). The events were relocated using the three-dimensional (3-D) seismic velocity model of *Hauksson* [2000] and the focal mechanisms determined using FPFIT [*Reasenberg and Oppenheimer*, 1985]. The focal mechanisms were inverted for stress orientation with the technique developed by *Michael* [1984, 1987]. The only methodological difference between the two studies was in how the earthquakes were spatially binned for inversion. A binning strategy is necessary so that there are enough subsets to detect spatial variation while each set has sufficient data to constrain the stress tensor.

[17] The binning method chosen by *Hardebeck and Hauksson* [1999] was hypothesis driven, designed to test the hypothesis that there is a stress rotation near the SAF. The bins were constructed on the basis of the location and orientation of the SAF, with long narrow bins centered on each fault segment and parallel bins on either side. *Hardebeck and Hauksson* [1999] tested for stress orientation differences between along-fault and far-field bins and reported a significant difference for most fault segments. They found a rotation from high angles (σ_H at 60°–100° to the SAF strike) far away (>50 km) from the SAF to lower angles (σ_H at 40°–50°) in the near field.

[18] *Townend and Zoback* [2001, 2004] chose a data-driven binning scheme, using square boxes on a fixed grid, iteratively subdividing each box if the local seismicity rate was high enough to contain at least 30 earthquakes in at least one subbox. Their inversion contains no information regarding the location or orientation of the SAF or any other geologic feature. Compiling the results of boxes at least partially within 10 km of the SAF, they report a stress orientation of 64° ± 14° (1σ) [*Townend and Zoback*, 2001] and 68° ± 7° [*Townend and Zoback*, 2004] near the fault, which they interpret as a high angle.

[19] *Townend and Zoback* [2001] attributed their disagreement with *Hardebeck and Hauksson* [1999] to the difference in binning technique, leading to differences in computed stress orientations. If this is true, it implies a flaw in one or both binning techniques, or it implies that the focal mechanism stress inversions are inherently unstable. *Townend and Zoback* [2001] asserted that the binning scheme used by *Hardebeck and Hauksson* [1999] was inconsistent with a homogeneous stress state over the spatial extent of the bin, a necessary assumption for inversion. The long narrow bins of *Hardebeck and Hauksson* [1999] combined earthquakes over large areas, possibly mixing events from different stress regimes. However, the larger boxes used by *Townend and Zoback* [2001] also mixed widely spaced events and additionally may have obscured signals related to the SAF by combining on-fault and off-fault events.

[20] The results of the two studies may be more similar than *Townend and Zoback* [2001] claimed. *Townend and Zoback*'s [2001] argument that the two sets of results are statistically significantly different was based on a comparison between their average orientation for all of southern California (64° ± 14°) and *Hardebeck and Hauksson*'s [1999] results for one specific segment near Fort Tejon (40°). This comparison may be flawed because the averaging done by *Townend and Zoback* [2001] was biased toward high seismicity rate areas, whereas the Fort Tejon area has a low seismicity rate. More importantly, the 40° observed at Fort Tejon is not inconsistent with a 64° ± 14° distribution, as many observations in a population will fall between 1 and 2 standard deviations from the mean. In fact, *Townend and Zoback* [2001] found an angle of ~50° in the box corresponding to the Fort Tejon segment, in agreement with *Hardebeck and Hauksson*'s [1999] observations to within the uncertainty of either measurement. *Hardebeck and Hauksson* [2001] also plotted the results of the two studies together on a profile across the Fort Tejon segment and found the two to be quite similar along the entire profile.

[21] We perform a more thorough comparison of the stress orientations from the two studies by comparing σ_H orientations on a 0.01°-spaced grid covering all of southern California. If a grid point falls within one of the inversion boxes of *Townend and Zoback* [2001], we assign the σ_H orientation of that box to that grid point. If the grid point does not fall inside a box, we do not interpolate and instead leave that grid point out of the comparison. We then find the distance to the nearest SAF segment and assign to the grid point the σ_H orientation that distance along the appropriate segment profile of *Hardebeck and Hauksson* [1999], again with no interpolation.

[22] For each grid point at which the σ_H orientation is defined in both models, we determine the angular difference between the two reported stress directions (Figure 2). The angles found by *Townend and Zoback* [2001] are on average slightly (≤10°) more clockwise (higher angle to the SAF) than those found by *Hardebeck and Hauksson* [1999]. This difference is not large enough to explain the difference in interpretation, as the low-angle and high-angle models differ by ~50°.

[23] For grid points within 100 km of the SAF the results of *Townend and Zoback* [2001] are oriented relatively more clockwise by 2.4° ± 14.5° (1σ) (Figure 2), and for grid points within 10 km of the fault they are oriented more

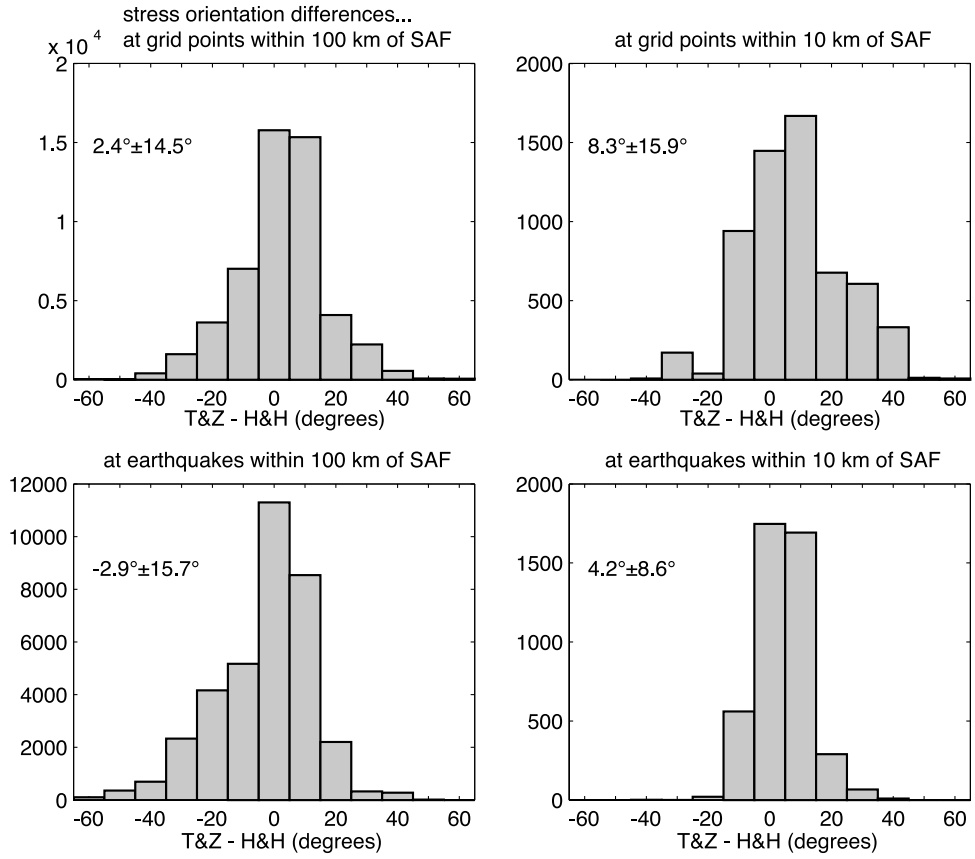

Figure 2. Histograms of the difference between the σ_H stress orientations determined by *Hardebeck and Hauksson* [1999] and *Townend and Zoback* [2001]. (top) Comparisons at points on a 0.01°-spaced grid that fall within 100 or 10 km of the SAF. (bottom) Similar comparisons at the locations of the earthquakes that comprise the focal mechanism data set. The difference is defined to be positive if the results of *Townend and Zoback* [2001] are relatively clockwise, corresponding to a higher angle to the SAF.

clockwise by 8.3° ± 15.9°. The larger difference near the fault may be because *Townend and Zoback*'s [2001] boxes obscure the SAF rotation by mixing near-fault and off-fault events. At the locations of the earthquakes used in the inversions, for events within 100 km of the SAF, the difference is −2.9° ± 15.7° (the results of *Hardebeck and Hauksson* [1999] are slightly more clockwise), and at the locations of events within 10 km of the SAF the difference is 4.2° ± 8.6°. The standard deviations of the difference histograms (9°–16°, Figure 2) are of comparable size to the inversion uncertainty, so much of the variability may be due to random error.

[24] The spatial pattern of the differences between the two models is shown in Figure 3. We focus on the boxes along the fault with high angular differences (Figure 4). All of these boxes contain regions in which the results disagree and regions in which they agree, and the earthquakes predominantly occur in the regions of agreement. *Hardebeck and Hauksson* [1999] and *Townend and Zoback* [2001] therefore find very similar stress orientations in areas where the stress field is sampled by earthquakes and differ only in how orientations are assigned to areas with little or no data. This can be thought of as a difference in smearing, with the binning technique of *Hardebeck and Hauksson* [1999] tending to smear along strike and the technique of *Townend and Zoback* [2001] tending to smear throughout the square boxes from seismicity that is often clustered in a small portion of the box. The smaller average difference in σ_H at earthquake locations, compared to all locations (Figure 2), also demonstrates the similarity of the two stress models in regions of sufficient data.

[25] The similarity of the stress orientations determined by *Hardebeck and Hauksson* [1999] and *Townend and Zoback* [2001] is encouraging, as it implies that focal mechanism stress inversion results are stable and reproducible. The major disagreement between *Hardebeck and Hauksson* [1999] and *Townend and Zoback* [2001] is in the interpretation of the observed orientations. In both studies, σ_H makes a 40°–65° angle with the SAF strike near the fault, not consistent with either the high-angle (∼80°) or low-angle (∼30°) model.

3.2. The Two New Inversions

[26] We perform two new inversions for stress orientation in southern California, following the philosophies of the hypothesis-driven and the data-driven inversions discussed in section 3.1. The first is a hypothesis-driven inversion designed to maximize the statistical power of the hypothesis test. The second is a data-driven inversion designed to bypass some of the potential drawbacks of the *Townend and Zoback* [2001] methodology. While the binning is done differently in each inversion, the tech-

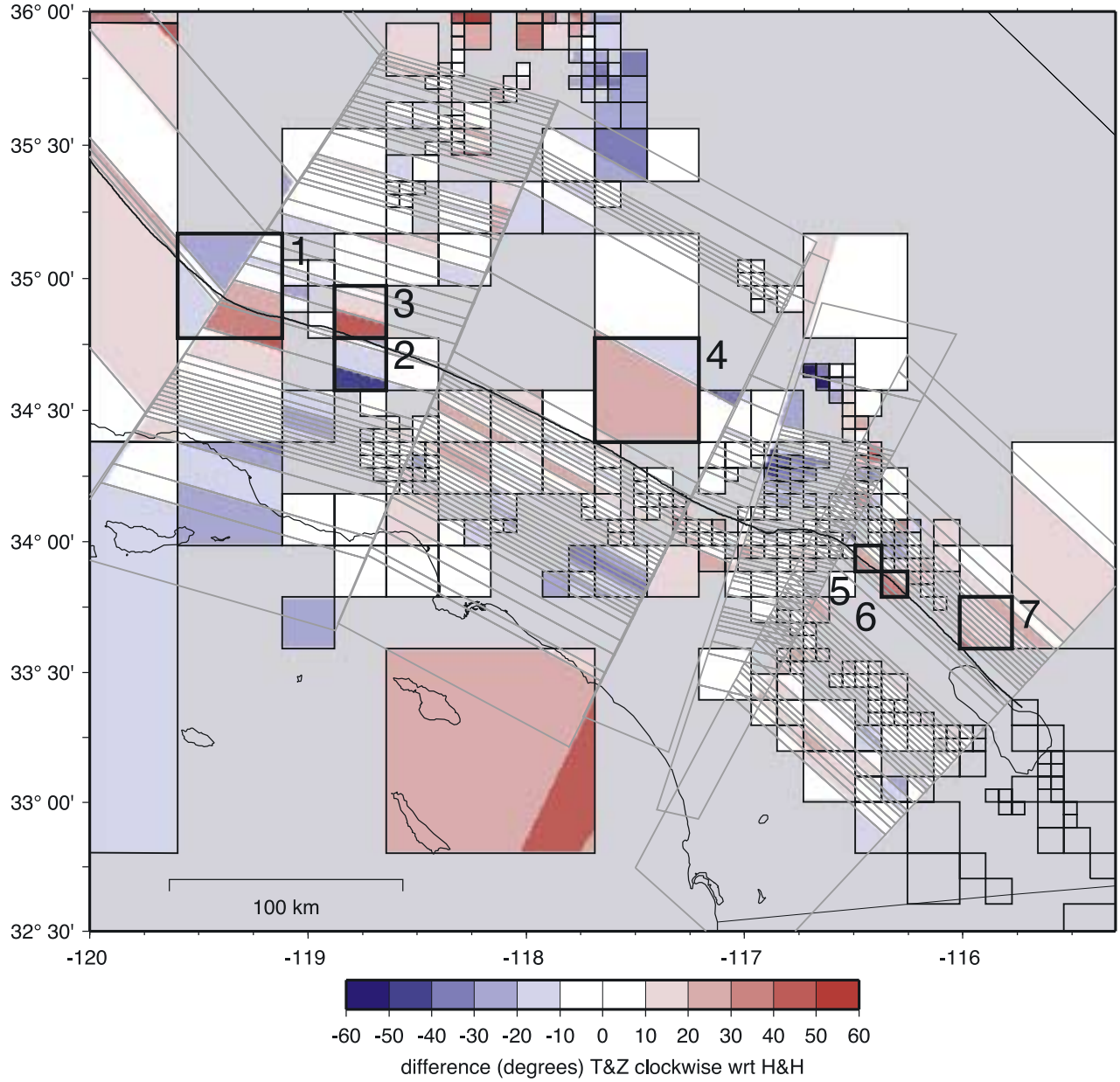

Figure 3. Map view comparison of the maximum compressive stress orientations found by *Hardebeck and Hauksson* [1999] and *Townend and Zoback* [2001]. For points on a 0.01° grid we find the distance to the nearest SAF segment and find the stress orientation at that distance from that segment in the profiles of *Hardebeck and Hauksson* [1999]. If the grid point falls within one of the inversion boxes of *Townend and Zoback* [2001], we find the orientation in that box; otherwise, we ignore that grid point and color it gray. No interpolation is performed for either model. Colors represent the difference in σ_H angle between the two models, red indicating that the *Townend and Zoback* [2001] orientation is relatively clockwise and hence at higher angle to the SAF. Black lines outline the boxes of *Townend and Zoback* [2001], and gray lines indicate the boxes of *Hardebeck and Hauksson* [1999]. Numbers indicate the boxes shown in close-up in Figure 4.

nique of *Michael* [1984, 1987] is used to invert the data in each bin. Uncertainty is estimated by repeated bootstrap resampling of the focal mechanism data set. The fault plane ambiguity is addressed by randomly selecting one of the nodal planes of each event for the initial inversion and again for each resampling. The uncertainty in the stress orientation therefore reflects the uncertainty in the choice of fault planes as well as the uncertainty in their orientations.

3.2.1. Hypothesis-Driven Inversion

[27] We wish to increase the statistical power of hypothesis tests concerning stress orientations relative to the SAF. Statistical power can be increased through data stacking (e.g., the stacking of seismograms). To create a stacked

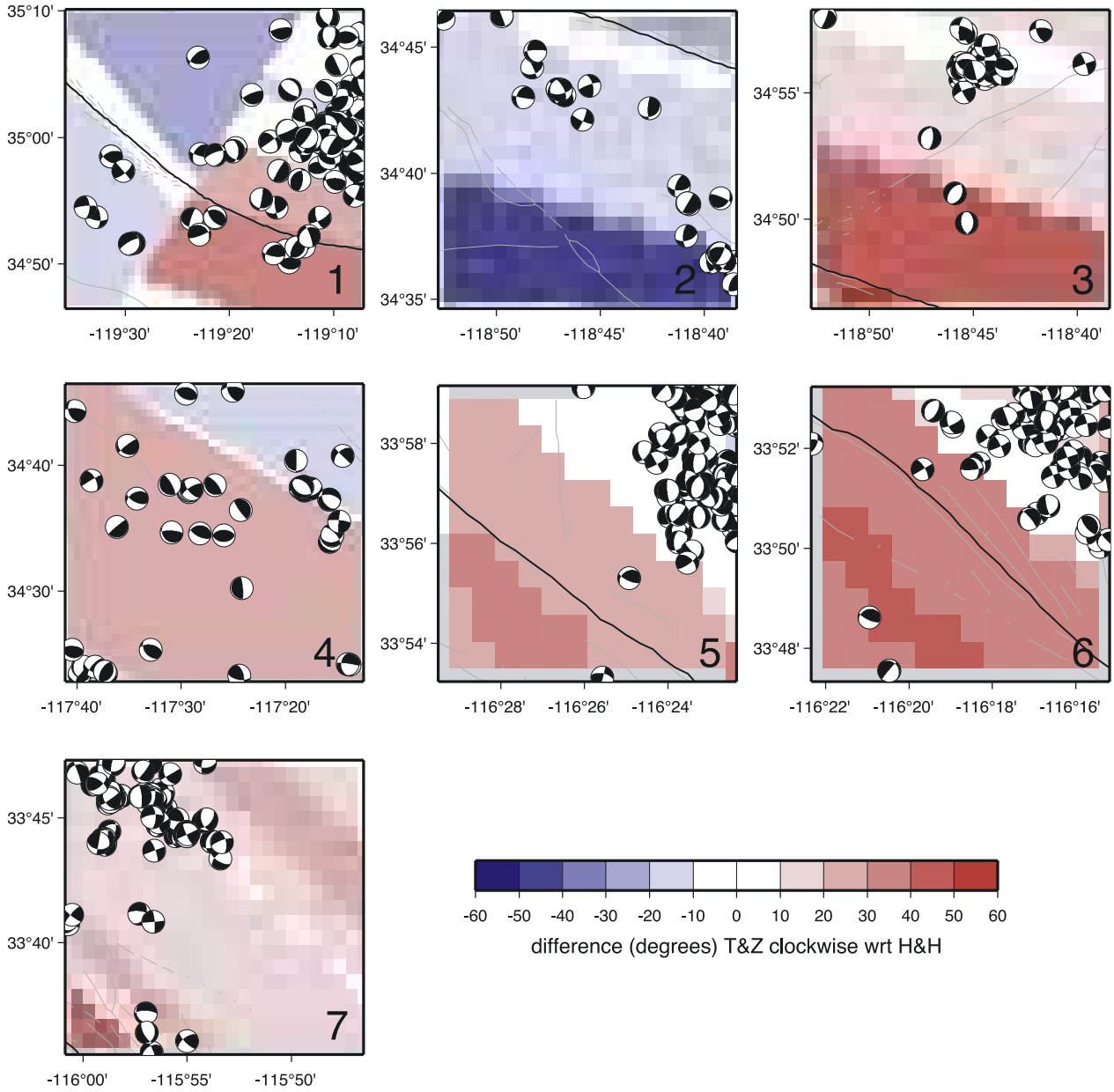

Figure 4. Close-up view of seven regions of Figure 3. These are the regions along the SAF showing the most disagreement between the σ_H stress orientations determined by *Hardebeck and Hauksson* [1999] and *Townend and Zoback* [2001]. Focal mechanisms are of the events from the data set used to invert for stress orientation.

stress orientation versus distance profile, we invert together the focal mechanisms from the entire length of the fault. We sort each event by its distance to the closest point on the SAF and rotate its focal mechanism by the strike of the SAF at that point, so that all orientations are with respect to the SAF strike. We then bin all the events on the basis of their perpendicular distance from the fault. All bins are at least 4 km wide and contain at least 200 events. We invert the rotated focal mechanisms in each bin for stress orientation relative to the SAF strike.

[28] Common signals with respect to the SAF should be amplified, while features of the stress field unrelated to the SAF will appear as noise and should cancel out. Additionally, we improve the quality of the inversion by using a new high-quality focal mechanism data set. The data set consists of ~8000 events recorded by the SCSN during 1981–2003, relocated using *Hauksson*'s [2000] 3-D velocity model. The focal mechanisms were determined using the technique of *Hardebeck and Shearer* [2002]. This data set is smaller than that used by *Hardebeck and Hauksson* [1999] and *Townend and Zoback* [2001] because the focal mechanisms meet a stricter quality criterion: They must be stable with respect to uncertainty in all of the input parameters including the seismic velocity model. All of the focal mechanisms have nodal plane uncertainty $\leq 35°$, and when many focal mechanisms are inverted together, the stress orientations may be even more tightly constrained than the individual mechanisms.

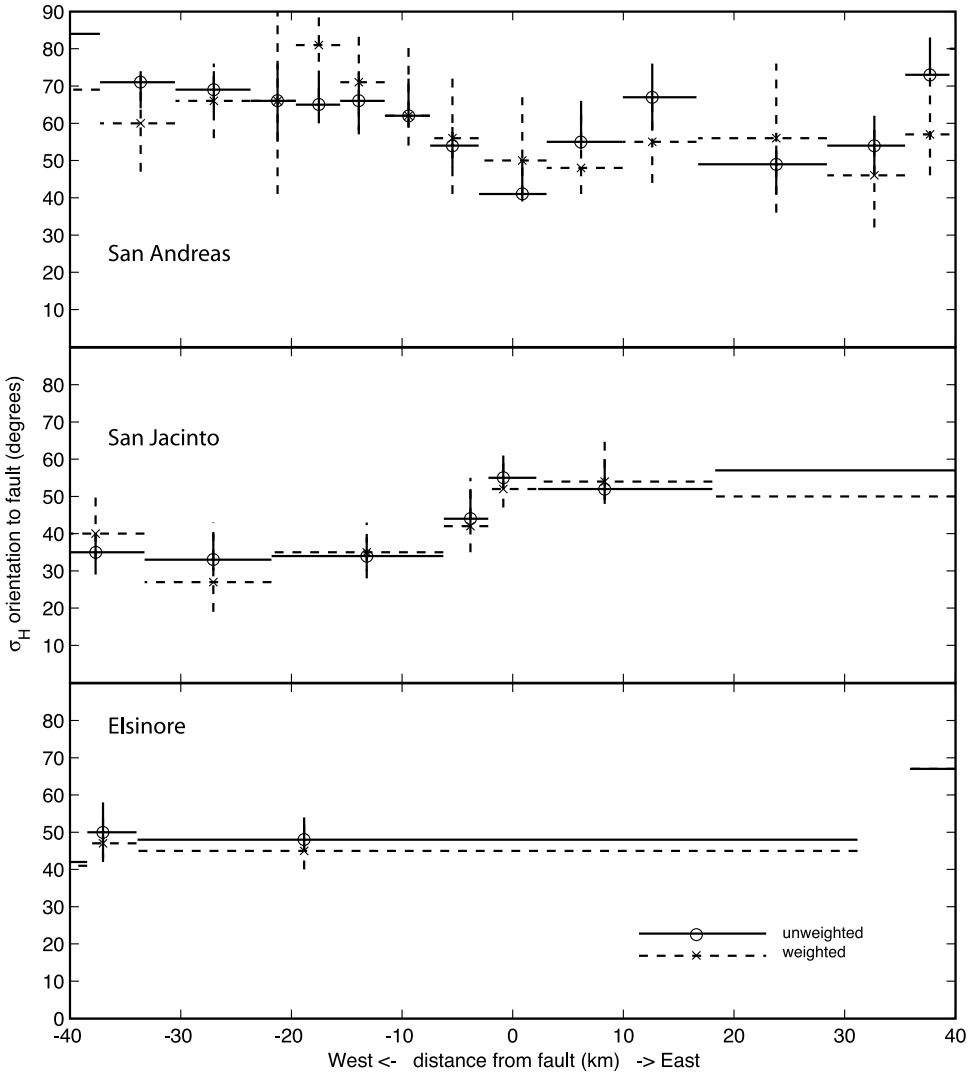

Figure 5. Orientation of the maximum horizontal compressive stress, σ_H, versus distance from the major faults of the SAF system in southern California for a stacked inversion of earthquake focal mechanisms. The earthquakes were binned by their distance from the closest point on the fault, and their mechanisms were rotated by the strike of the fault at that point. Events in each distance bin were inverted for stress orientation relative to the fault strike (solid lines). Events were also weighted in the inversion inversely proportionally to the local seismicity rate, so that areas with high seismicity rate do not dominate the inversion (dashed lines). Horizontal lines indicate the spatial extent of the bins; vertical lines indicate the 1σ uncertainty of the inversion result. The orientation of σ_H is $\sim$40°–55° to the strike at the SAF, $\sim$55° at the San Jacinto, and $\sim$50° at the Elsinore.

Although there are fewer total mechanisms than in *Hardebeck and Haukssons*'s [1999] study, the stacking of multiple profiles allows us to achieve similar spatial resolution in the fault normal direction.

[29] The seismicity rate is not constant along strike, so the results of the stacked inversion could be biased to the high-seismicity areas. Analogous to seismogram stacking where one normalizes the traces so that high-amplitude records do not dominate the result, we normalize by seismicity rate by applying a weight to each focal mechanism in the inversion. The weight is inversely proportional to the number of earthquakes in the data set in a 10 $\times$ 10 km region around the event.

[30] For both the weighted and unweighted inversions (Figure 5), σ_H is at intermediate angle to the SAF strike near the fault, 42° ± 5° for the unweighted inversion and 55° ± 13° for the weighted inversion. We perform inversions for two other major faults of the San Andreas system in southern California (Figure 1), where σ_H also makes an intermediate angle to the fault strike: 58° ± 4° unweighted and 54° ± 6° weighted for the San Jacinto fault and 52° ± 5° unweighted and 48° ± 7° weighted for the Elsinore fault.

[31] Stress orientations cannot be obtained from a single focal mechanism or a set of identical mechanisms, so a diversity of mechanisms is required. *Hardebeck and Hauksson* [2001] found that a good measure of mechanism diversity is the RMS angular difference from the mean mechanism. Accurate inversion results can be found for high-quality data sets if the RMS difference is $\geq$30° and for

noisy data sets if the RMS difference is $\geq 40°-45°$. The RMS difference for events in the bin on the SAF is 46°, so there is clearly adequate focal mechanism diversity for this inversion.

[32] The misfit of the focal mechanisms near the SAF to the best fit stress tensor is consistently around 40°. This misfit indicates that the inversions are likely to have successfully identified the homogeneous part of the stress tensor [*Michael*, 1991], but it is at the high end of the acceptable misfit range and implies significant heterogeneity in the stress field. The misfit is similar if the focal mechanisms are not first rotated relative to the fault strike. Many of the earthquakes along the SAF are clustered in the San Bernardino region east of Cajon Pass, and the misfits for both the rotated and nonrotated inversions are dominated by the heterogeneity of this cluster of events. Additional misfit may be due to the nodal plane ambiguity.

[33] The rotation to high angle in the far field reported by *Hardebeck and Hauksson* [1999] does not appear to be a stable feature of the profiles. Although a rotation to higher angle is observed west of the SAF (Figure 5), it is less pronounced to the east and is not observed across the San Jacinto or Elsinore faults. The stability of the intermediate angle in the near field suggests that the stress near the fault is controlled by the fault. The stress in the far field may be primarily controlled by other factors and may not have a consistent orientation relative to the fault. Thus a stress rotation occurs if the far- and near-field stress orientations are different but does not occur where they are similar.

3.2.2. Data-Driven Inversion

[34] We devise an alternative data-driven binning algorithm that addresses several deficiencies with the fixed-grid boxes used by *Townend and Zoback* [2001]. With their algorithm it is possible for the larger bins to include multiple clusters of events that are spatially quite far apart or for closely grouped clusters of earthquakes to be split between multiple bins. Their binning scheme also omits from the inversion all of the earthquakes falling in subareas with too few data for inversion. Instead of using a predefined grid we bin the earthquakes using cluster analysis. We use the same focal mechanism data set as *Hardebeck and Hauksson* [1999] and *Townend and Zoback* [2001]. The new data set is not used because it is too small for detailed spatial coverage of the region.

[35] We begin by defining each earthquake as a separate cluster, and then we iteratively combine the two spatially closest clusters. We define cluster location as the average location of the earthquakes that compose it, and we define distance as Cartesian distance in the horizontal plane, ignoring event depth because of its relatively greater uncertainty. We stop clustering when the clusters contain enough events for inversion, so we impose a rule that two clusters are not combined if both contain at least 30 earthquakes.

[36] The spatial extent of the resulting clusters and the σ_H orientations obtained from inverting the focal mechanisms of each cluster are shown in Figure 6. For clusters within $\sim$10 km of the SAF the angle of σ_H relative to the fault varies from $\sim$20° to $\sim$80°, with an average and standard deviation of 55° ± 22°, overlapping the range found by *Townend and Zoback* [2000]. This demonstrates the general stability of the stress orientations with respect to the details of the binning scheme. The events used in these inversions are on average 6 km from the SAF, farther than the events in the stacked inversion, which are $\leq$2 km from the fault. The inclusion of more distant earthquakes in many of the near-fault clusters accounts for the higher average angle.

4. Stress Orientations in Northern California

4.1. Comparison of Previous Studies

[37] We compare the stress orientations presented by *Townend and Zoback* [2001, 2004] and *Provost and Houston* [2003] for three locations in the San Francisco Bay Area. The comparison is not as straightforward as for southern California because the two studies did not use the same data set or inversion technique. Additionally, *Townend and Zoback* [2001] focused on just the three local areas, while *Provost and Houston* [2003] took a more regional approach.

[38] *Townend and Zoback* [2001, 2004] present a new inversion of 28 earthquakes near the SAF west of San Jose. They found σ_H at 84° to the fault strike. The spatial extent of their data set is roughly equivalent to three spatial bins of *Provost and Houston* [2003] (bins BAc2, BAc3, and BAc5), and the data span a similar time period. The average σ_H orientation of the three bins is 86° to the SAF, consistent with the results of *Townend and Zoback* [2001]. This again demonstrates the stability of focal mechanism stress inversion results. Although the σ_H orientations near the SAF found by the two studies are very similar, their interpretations are different because of the different scope of the studies. The *Provost and Houston* [2003] study covered the entire SAF system in northern California, and in this context the high σ_H angle near San Jose is clearly an anomaly.

[39] *Townend and Zoback* [2001] also revisit results from previous studies of two aftershock sequences. The σ_H orientations found for these sequences are rotated clockwise (higher angle to the SAF) by up to 25° compared to the orientations at the same locations found from events spanning 1969–2000 [*Provost and Houston*, 2003]. The Loma Prieta region shown by *Townend and Zoback* [2001] roughly corresponds to eight bins of *Provost and Houston* [2003] (BAs6, BAs9-BAs15). The aftershocks imply σ_H at 77° to the SAF [*Townend and Zoback*, 2001; *Zoback and Beroza*, 1993], while *Provost and Houston* [2003] found an average σ_H orientation of 60° to the SAF. The Morgan Hill region corresponds to three on-fault and four off-fault bins of *Provost and Houston* [2003]. While the aftershocks imply σ_H at 72°–78° to the SAF [*Townend and Zoback*, 2001; *Oppenheimer et al.*, 1988], the average orientation in *Provost and Houston*'s [2003] on-fault bins (BAs36, BAs39, and BAs41) is 53°, and the average of the off-fault bins (BAs33, BAs38, BAs40, and BAs43) is 67°.

[40] The difference may be due to atypical stress orientations during the aftershock sequences. Main shocks have been shown to alter the stress orientations near the fault [e.g., *Hauksson*, 1994; *Hardebeck and Hauksson*, 2001], and aftershocks have been shown to respond to the main shock-induced stresses [e.g., *King et al.*, 1994]. Therefore the stress orientations found from aftershock sequences may not be indicative of the long-term background stress field. At Loma Prieta the main shock altered the stress field and rendered it too heterogeneous for

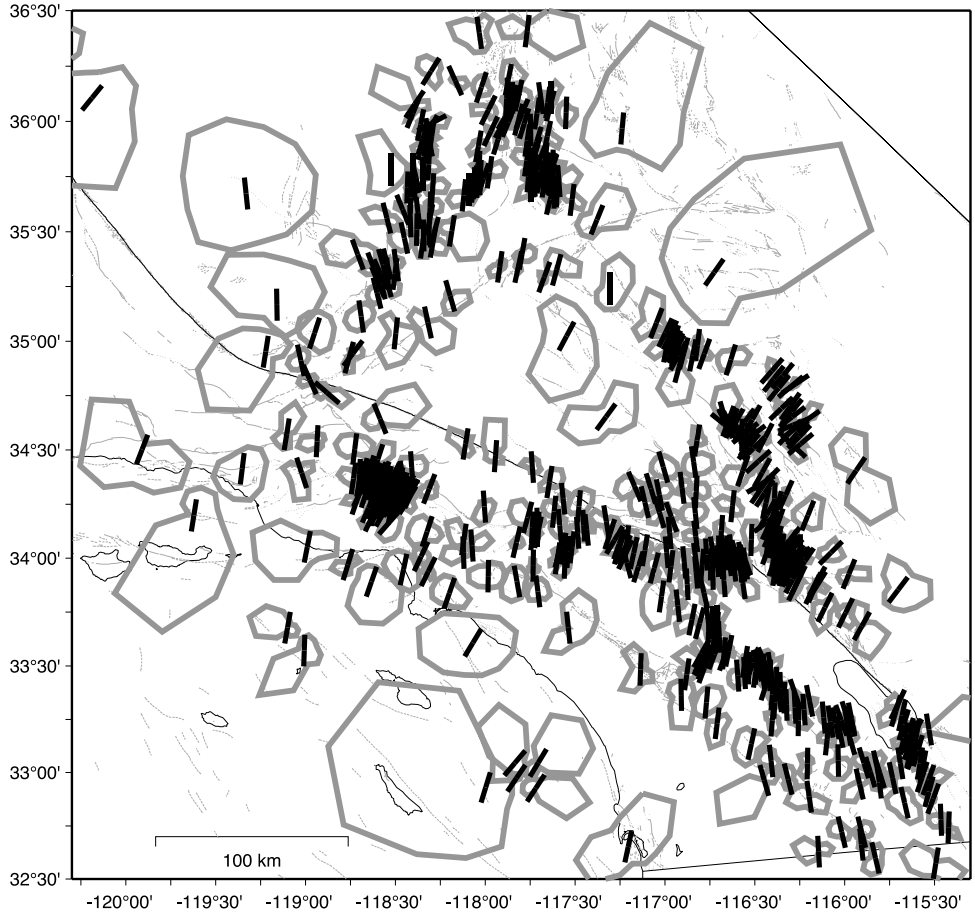

Figure 6. Stress orientations in southern California determined from earthquakes grouped together using cluster analysis. Gray lines outline the approximate spatial extent of the clusters, while the black bars indicate the orientation of the maximum horizontal stress axis, σ_H. The bars are located at the average location of events in the cluster. The σ_H axis for the clusters within 10 km of the SAF make a 55° ± 22° angle to the strike.

inversion [*Michael et al.*, 1990; *Michael and Eberhart-Phillips*, 2000]. At Morgan Hill, however, no coseismic change in stress was observed.

[41] Because of the longer time span of the data set we take the results of *Provost and Houston* [2003] to be more indicative of the background σ_H orientation to the SAF. They found σ_H along major faults of the SAF system typically oriented at 40°–60° to the fault strike, similar to the intermediate angles seen in southern California.

4.2. Two New Inversions

[42] We perform two new inversions for stress orientation in northern California, using the same hypothesis-driven inversion and data-driven inversion techniques used for southern California. For both new inversions we use a data set of ~28,000 earthquakes recorded during 1969–2003 by the Northern California Seismic Network (NCSN), all of which occur north of the north end of the creeping section at San Juan Bautista. The NCSN catalog locations were used, and focal mechanisms were computed using the technique of *Hardebeck and Shearer* [2002]. This data set meets the same quality criteria as the southern California catalog, and all mechanisms have nodal plane uncertainty ≤35°.

[43] The focal mechanisms of events along faults in northern California may be biased because of lateral refractions [e.g., *Oppenheimer et al.*, 1988; *Ben-Zion and Malin*, 1991]. If there is a significant velocity contrast across the fault, the first arrival at stations on the slow side of the fault may be a wave traveling through the fast medium, not the direct wave as assumed. If lateral refractions affect our focal mechanism data set, we would expect to see a higher rate of erroneous focal mechanisms along faults with greater velocity contrasts. However, the focal mechanisms of events along faults with high velocity contrasts are just as consistent with the fault orientation as the focal mechanisms of events on other faults (D. Kilb and J. L. Hardebeck, Fault parameter constraints using relocated earthquakes: A validation of first motion focal mechanism data, manuscript in preparation, 2004). Therefore there is no evidence that our data set is biased by lateral refractions.

4.2.1. Hypothesis-Driven Inversion

[44] We find a stacked stress orientation versus distance profile across the SAF in northern California by inverting the entire data set together. Events are sorted by distance to the fault, and the focal mechanisms are rotated relative to the fault strike. The orientation of σ_H near the locked portion of the SAF is at intermediate angle to the fault strike

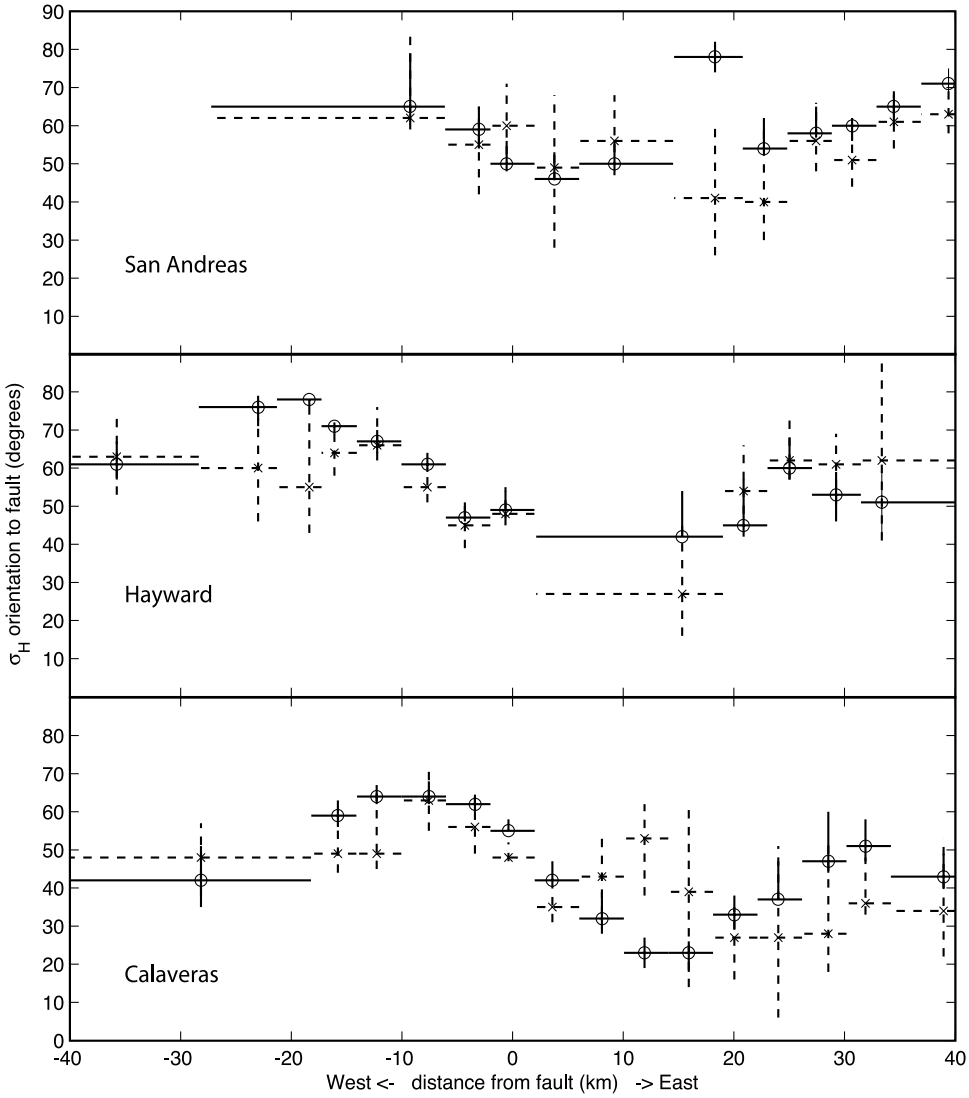

Figure 7. Orientation of the maximum horizontal compressive stress, σ_H, versus distance from the faults of the SAF system in northern California for a stacked inversion of earthquake focal mechanisms. The earthquakes were binned by their distance from the closest point of the fault, and their mechanisms were rotated by the strike of the fault at that point. Events in each distance bin were inverted for stress orientation relative to the fault strike (solid lines). Events were weighted in the inversion inversely proportionally to the local seismicity rate, so that areas with high seismicity rate do not dominate the inversion (dashed lines). Horizontal lines indicate the spatial extent of the bins; vertical lines indicate the 1σ uncertainty of the inversion result. The σ_H angle makes a $\sim 50^\circ - 60^\circ$ angle to the strike on the SAF, a $\sim 50^\circ$ angle on the Hayward, and a $\sim 50^\circ - 55^\circ$ angle on the Calaveras.

for both weighted and unweighted inversions (Figure 7). The unweighted inversion finds σ_H at $51^\circ \pm 3^\circ$, and the weighted inversion finds σ_H at $61^\circ \pm 12^\circ$.

[45] We also perform inversions for two other major faults of the San Andreas system in the San Francisco Bay Area, the Hayward fault and the Calaveras fault (Figure 1). For these faults, σ_H also makes an intermediate angle to the fault strike: $49^\circ \pm 4^\circ$ unweighted and $48^\circ \pm 5^\circ$ weighted for the Hayward fault and $55^\circ \pm 2^\circ$ unweighted and $48^\circ \pm 3^\circ$ weighted for the Calaveras fault.

[46] As in southern California, the misfit of the focal mechanisms near the SAF to the best fit stress orientation is consistently around 40°, indicating that the homogeneous part of the stress tensor was found [*Michael*, 1991]. The misfit also implies significant local heterogeneity in the stress field. The misfit is similar if the focal mechanisms are not first rotated relative to the fault strike, but since the fault strike does not vary much in northern California, this is not surprising. The RMS difference from the mean mechanism is 33°, indicating that there is enough focal mechanism diversity to obtain a good inversion result, assuming this is a high-quality data set [*Hardebeck and Hauksson*, 2001].

4.2.2. Data-Driven Inversion

[47] We bin the northern California focal mechanism catalog using cluster analysis and invert for the stress

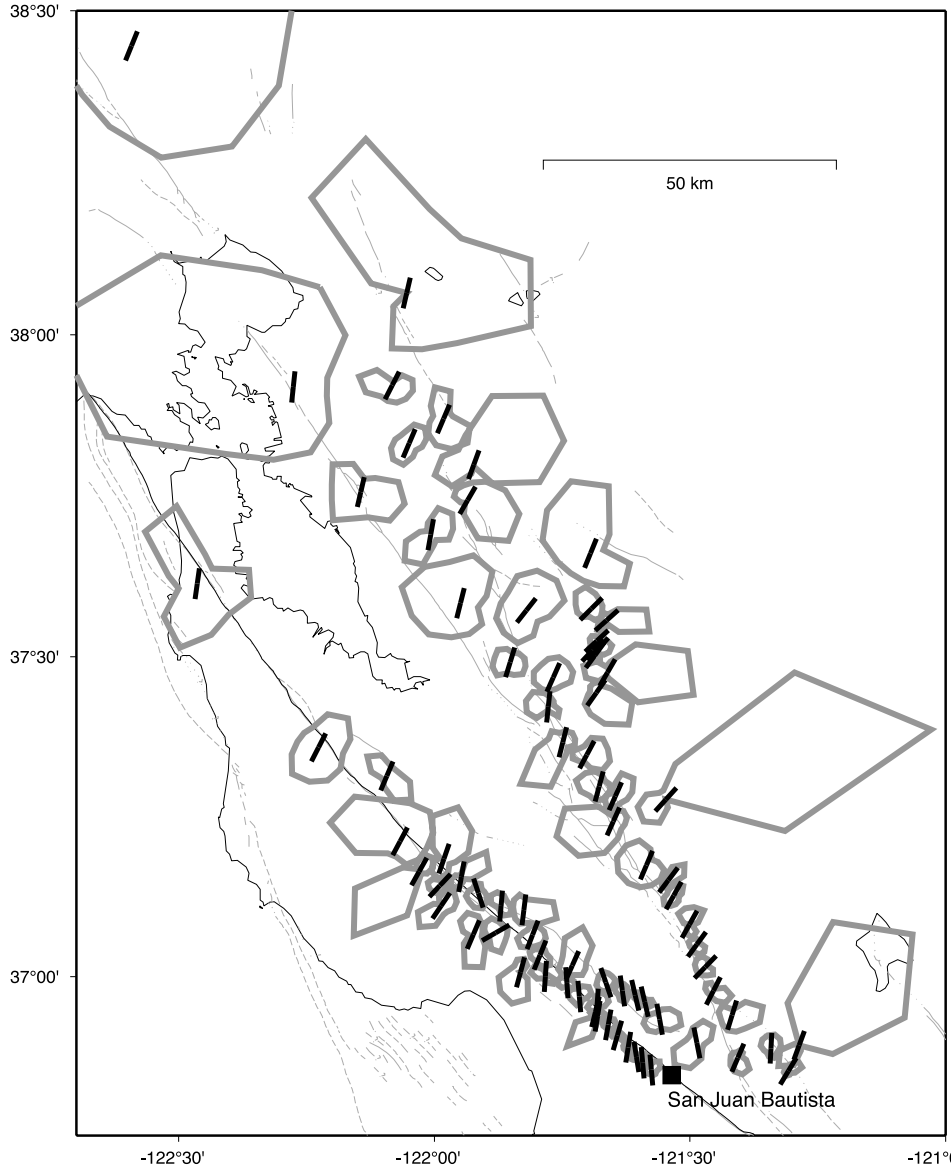

Figure 8. Stress orientations in northern California determined from earthquakes grouped together using cluster analysis. Gray lines outline the approximate spatial extent of the clusters, while the black bars indicate the orientation of the maximum horizontal stress axis, σ_H. The bars are located at the average location of event in the cluster. The σ_H axis for clusters within 10 km of the SAF makes a 55° ± 19° angle with the strike.

orientation in each cluster (Figure 8). For clusters within 10 km of the locked portion of the SAF (north of San Juan Bautista), the angle of σ_H relative to the fault is 55° ± 19° (1σ), similar to the along-fault angles of 40°–60° found by *Provost and Houston* [2003]. The average distance of the events from the SAF is 3 km, and the results are similar to the stacked inversions using events ≤2 km from the SAF.

5. Stress Orientations Along the Creeping Section

[48] The central section of the SAF between Parkfield and San Juan Bautista is unusual in that it appears to accommodate almost its entire slip rate in creep. The creeping segment (Figure 1) is also atypical in that the σ_H orientation is consistently at high angle (80°–90°) within ~20 km of the SAF [*Provost and Houston*, 2001]. The high σ_H angle in the near field implies that the relatively weak fault model may be appropriate for the creeping section. Creep also suggests a low strength for this segment of the SAF.

[49] The only exception to the high σ_H angle is in a <1–3 km wide zone along the fault, where σ_H is oriented 45°–55° to the fault strike [*Provost and Houston*, 2001]. This may be an artifact of inverting sets of on-fault events with nearly identical focal mechanisms, which do not fully sample the stress tensor. Alternatively, *Rice* [1992] has proposed a model for a weak-fault zone containing fluids at high pressures, which predicts a rotation of σ_H to low angles within the narrow fault core. The observations of *Provost and Houston* [2001] suggest that the creeping

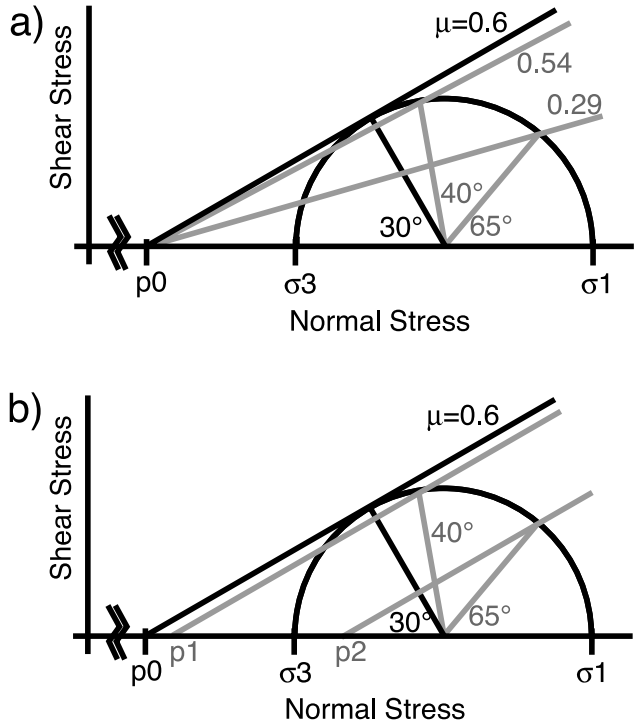

Figure 9. Mohr circle diagrams for the intermediate-strength San Andreas model. The surrounding crust is assumed to be strong ($\mu = 0.6$) and at critical stress. The failure envelope for $\mu = 0.6$ and the orientation of the optimal failure plane are shown in black. The gray lines show the location on the Mohr circle for faults at 40° and 65° to the σ_1 axis and the failure envelopes for these faults. (a) Pore pressure in the fault is assumed to be the same as in the surrounding crust (p_0), and the coefficient of friction varies from $\mu = 0.29$ to 0.54. (b) Assuming $\mu = 0.6$, the pore pressure varies from $p_1 = p_0 + 0.12(\sigma_3 - p_0)$ for a fault at 40° to $p_2 = \sigma_3 + 0.32(\sigma_3 - p_0)$ for a fault at 65°.

section may be very weak and creeping because of elevated fluid pressure.

6. Discussion

[50] Neither the high-angle, relatively weak fault model nor the low-angle, strong-fault model satisfactorily describes the locked segments of the SAF, where σ_H is most often at intermediate angle to the fault strike. The strong-fault model is still viable, however, if the San Andreas is assumed to be a preexisting plane of weakness which fails despite being nonoptimally oriented for failure. This is possible if the orientation of σ_H is less than the lockup angle (~60°) at which it becomes more favorable for a new fault to form than for an old one to slip.

[51] Alternatives to the strong- and relatively weak fault models are needed. We will discuss an intermediate-strength SAF model on the basis of the assumption that all other faults are strong, and we will discuss a low-stress model on the basis of the assumption that all faults are weak. We will also review more sophisticated numerical models. Since all the faults of the SAF system exhibit similar stress orientations, these models potentially apply to all of these faults (San Jacinto, Elsinore, Hayward, and Calaveras), not just the SAF.

6.1. Intermediate-Strength SAF Model

[52] One possible model is that of an intermediate-strength SAF, corresponding to the intermediate angle of σ_H to the fault strike. We constrain the SAF strength for this model by assuming that all other faults are strong, consistent with laboratory rock friction experiments, and that the crust is critically stressed with hydrostatic pore pressure, consistent with observations in deep boreholes [*Townend and Zoback*, 2001]. This information, along with the orientations and relative magnitudes of the principal stress axes, completely defines the stress tensor. Given the full stress tensor, the orientation of the SAF with respect to the stress axes is a direct measure of the stress on the fault and therefore its strength.

[53] We compute the frictional strength at seismogenic depths, equivalent to the shear stress on the fault, using a Mohr circle construction (Figure 9). The construction assumes that the SAF is in a strike-slip to transpressional tectonic regime [e.g., *Hardebeck and Hauksson*, 2001; *Provost and Houston*, 2003], with the maximum compressional stress axes, σ_1, horizontal, and the vertical axis σ_2 equal to the overburden pressure. In a pure strike-slip regime, with intermediate stress axis $\sigma_2 = (\sigma_1 + \sigma_3)/2$, the fault strength is 65–85 MPa at 10 km depth, and in a transpressional regime, $\sigma_2 = \sigma_3$, the fault strength is 130–165 MPa. This is comparable to the 75–145 MPa strength of strong fault, $\mu = 0.6$, at 10 km depth.

[54] This model shares a problem with the strong-fault model because it predicts significant frictional heating, but no evidence of this heating has been found [*Brune et al.*, 1969; *Lachenbruch and Sass*, 1992; *d'Alessio et al.*, 2003]. However, because the frictional heating occurs only during earthquake slip, it is the dynamic frictional resistance that must be low. If the SAF were to weaken significantly during rupture [e.g., *Melosh*, 1996; *Andrews and Ben-Zion*, 1997], this would result in lower frictional heating.

[55] We assume that fluid pressure in the SAF zone is at hydrostatic pressure and estimate the coefficient of friction of the SAF using a Mohr circle construction (Figure 9a). The coefficient of friction for the SAF ranges from $\mu = 0.29$ for σ_H (=σ_1) at 65° to $\mu = 0.54$ for σ_H (=σ_1) at 40°.

[56] We can alternatively assume that the SAF has $\mu = 0.6$ but is of intermediate strength because of increased fluid pressure in the fault zone, which reduces the effective normal stress. The required pore pressure is found using a Mohr circle construction (Figure 9b). The pore pressure ranges from 110% of hydrostatic for σ_H at 40° to 230% of hydrostatic for σ_H at 65°, assuming a strike-slip regime, and from 120% hydrostatic for σ_H at 40° to 360% hydrostatic for σ_H at 65°, assuming transpression. Most of the range of possible pore pressure values is lower than the minimum principal stress and the lithostatic pressure, but the high end of the range exceeds these values.

[57] Low-permeability barriers due to mineralization can maintain high fault zone pore pressures. Evidence for this has been observed in the field [*Chester et al.*, 1993] and in the laboratory [*Blanpied et al.*, 1992]. In the model proposed by *Rice* [1992], fluids are constantly fed from the

lower crust into a relatively permeable fault zone core surrounded by low-permeability barriers. *Rice* [1992] also proposed that stress is higher in the fault zone, preventing hydrofracture due to the high fluid pressure. In an alternative cyclical model [*Sibson*, 1992; *Byerlee*, 1993; *Sleep and Blanpied*, 1992], low-permeability barriers seal fluids into the fault, interseismic fault zone compaction raises the pore pressure, and coseismic fracturing increases porosity and decreases pore pressure.

6.2. Low-Stress Crust Model

[58] An alternative model for fault strength is suggested by the observation that large earthquakes are capable of altering the local stress field. For example, the 1992 *M*7.3 Landers, California, earthquake rotated the σ_H axis orientation by 10°–20° [*Hauksson*, 1994; *Hardebeck and Hauksson*, 2001], and the 1989 *M*7.0 Loma Prieta earthquake completely relieved the homogeneous part of the stress field [*Michael et al.*, 1990]. An earthquake could significantly affect stress orientations only if the stress drop were on the same order of magnitude as the background deviatoric stress. Average earthquake stress drop is typically estimated to be on the order of ~10 MPa, compared to the ~100 MPa deviatoric stress at seismogenic depths required if the majority of faults are strong and the crust is critically stressed. Therefore several studies have concluded that the background deviatoric stress must be low, on the order of tens of megapascals [*Yin and Rogers*, 1995; *Hardebeck and Hauksson*, 2001]. These results apply to the average stress magnitude on the length scale of the main shock rupture, ~70 km. Small-scale strength heterogeneity, with localized patches of high stress, for instance, at crack tips, may also be present.

[59] In this model all active faults must be weak in order to fail at low applied shear stress, with frictional strength on the order of the earthquake stress drop, ~10 MPa (Table 1). Fault weakening may be due to either low (<0.1) coefficient of friction or high (approximately lithostatic) pore fluid pressure. There is some evidence that major faults, in general, are weak. For instance, the prerupture shear stress on the main shock fault plane of the 1995 Kobe, Japan, earthquake appears to have been low [*Spudich et al.*, 1998], so the fault must have been weak for the earthquake to have occurred.

[60] If the deviatoric stress magnitude were on the order of earthquake stress drops, the orientation of σ_H to the fault strike would vary throughout the seismic cycle. Immediately following the (nearly) total stress drop of an earthquake, the σ_H axis would be (nearly) perpendicular to the fault strike. This is consistent with the unusually high σ_H angles found for some aftershocks sequences, discussed in the comparison of observed stress orientation in northern California. Shear stress would build on the fault during the interseismic period, causing the σ_H axis to rotate to lower angles, with a minimum of 45°. In contrast to the case of a high-stress crust the orientation of σ_H to the fault would be indicative of the loading state of the fault, not its strength. The intermediate angles along the SAF are consistent with the lack of recent major earthquakes.

[61] The low-stress model appears to contradict observations of high deviatoric stress in deep boreholes [e.g., *Brudy et al.*, 1997; *Townend and Zoback*, 2000]. However, all deep (>4 km) observations to date come from intraplate areas. It is possible that the upper crust is at lower strength in plate boundary regions. The low-stress model is also consistent with the presence of mountains in the plate boundary region. To isostatically support 2 km high mountains, on a 30 km thick crust, requires a force of 2×10^{12} N/m per unit length along the range front. If the mountains are supported solely by the crust, the resulting deviatoric stress is ~30 MPa, and if they are supported over the entire lithosphere, the deviatoric stress is only ~15 MPa. This deviatoric stress is consistent with either a weak or a strong crust.

6.3. Numerical Models

[62] We compare the observed stress orientations to more sophisticated theoretical and numerical models of fault behavior that contain predictions for stress orientations near the SAF. These models reveal that while the connection between fault strength and stress orientation is not as simple as framed by the strong-fault versus weak-fault debate, most models are roughly equivalent to a simple weak, intermediate, or strong SAF.

[63] *Scholz* [2000] presented a model of the SAF as a locked fault over a localized ductile shear zone. The crust on either side of the fault was assumed to be strong, including thrust faults striking parallel to the SAF. The system was loaded by SAF parallel shear and fault normal compression. The model predicts $\mu \approx 0.6$ for the SAF, assuming hydrostatic pore pressure, which is clearly a strong-fault model. The model predicts a σ_H rotation from ~90° in the far field to ~40° near the SAF, as observed at Fort Tejon [*Hardebeck and Hauksson*, 1999]. This model was specifically designed for the Fort Tejon segment, which is under more fault normal compression than most segments of the SAF because of its oblique orientation relative to the plate motion. Therefore the model may not directly apply to other segments.

[64] *Chéry et al.* [2001] present a finite element model of the SAF in central and northern California. The crust is modeled as an elastic layer over a viscoelastic layer. The surrounding crust is assumed to be strong ($\mu = 0.6$), while the fault itself is very weak ($\mu = 0.05$) or somewhat weak ($\mu = 0.18$). The system is loaded from the side by fault parallel motion and a small component of fault normal compression, consistent with the local tectonics. Not surprisingly, the case of the very weak SAF, analogous to the relatively weak SAF model, predicts high σ_H angles (65°–90°). This model is appropriate for the creeping section of the SAF, as *Chéry et al.* [2001] discuss, but not for other segments. The somewhat weak fault model, more similar to the simple intermediate-strength SAF model proposed in section 6.1, predicts intermediate σ_H angles (50°–60°) more consistent with those observed along the locked portions of the fault.

[65] *Lynch and Richards* [2001] also present a finite element model of a planar fault in an elastic layer over a viscoelastic layer, also loaded by fault parallel and some fault normal motion at the boundaries of the model. The fault strength is equivalent to $\mu < 0.1$, or a very weak fault, and results in a fairly high (>60°) angle of σ_H to the fault in accordance with the relatively weak fault model. They also find that restricting deformation in the lower crust to a finite width shear zone can result in a rotation of stress orientations to lower angles near the fault, consistent with

the observations of *Hardebeck and Hauksson* [1999] and *Provost and Houston* [2003].

[66] *Fitzenz and Miller* [2004] present a model of the SAF in southern California around Fort Tejon, the location of a significant change in fault strike. They model the SAF north and south of the bend as frictional surfaces with μ = 0.6 containing sealed fluid cells that may be at high pressure because of interseismic fault compaction. The strength of the model faults is variable owing to interseismic and coseismic changes in pore pressure. The surrounding crust is modeled as an elastic half-space loaded by fault parallel shear at the base of the seismogenic zone and compression in the far field orthogonal to the northern fault segment.

[67] The *Fitzenz and Miller* [2004] model produces deviatoric stresses at seismogenic depths consistent with a strong crust. The model predicts a σ_H orientation of 45°–55° to the SAF strike in a 20 km wide zone along the fault, consistent with the intermediate angles typically observed. Heterogeneity in cumulative slip may locally rotate the stress field by up to ~30°, meaning that there are locations where σ_H is at high (~80°) or low (~30°) angles to the fault, consistent with the observed variability in stress orientation along the strike of the SAF. The *Fitzenz and Miller* [2004] model appears to be a more sophisticated version of the simple model of an intermediate-strength SAF with elevated pore fluid pressure and demonstrates that such a model can explain the along-strike variability of the observed stress field, as well as the typical intermediate orientations.

7. Conclusion

[68] The strength of the SAF and the orientation of stress in its vicinity are controversial. Two end-member models have been proposed: the strong-fault model (in which the SAF frictional strength is equivalent to laboratory samples) and the relatively weak fault model (in which the SAF is an order of magnitude weaker than the surrounding crust). These two models imply that the maximum horizontal compressive stress axis, σ_H, should be at low angle (~30°) or at high angle (~80°) to the fault strike, respectively.

[69] Several recent studies have attempted to test these models by inverting the focal mechanisms of small earthquakes for stress orientation near the SAF but are inconsistent as to which model is supported. Particularly at odds are two studies in southern California [*Hardebeck and Hauksson*, 1999, 2001; *Townend and Zoback*, 2001, 2004] that use the same focal mechanism data set but reach opposite conclusions as to whether σ_H is at high or low angle to the SAF. *Townend and Zoback* [2001] proposed that the difference arises from the use of different schemes for spatially binning the seismicity for inversion. We test this idea by comparing the results of the two studies over the entire region and find that the stress orientations are actually very similar. The largest differences occur in regions with few earthquakes, as the two techniques mainly differ in how stress orientations are assigned to the areas between earthquake clusters. We also find that two studies of northern California [*Townend and Zoback*, 2001; *Provost and Houston*, 2003], which reported differences in stress orientation, also agree where similar data are used. Where the two disagree, *Townend and Zoback* [2001] had based their results on aftershocks, which may be responding to stress perturbations from the main shock, especially at Loma Prieta.

[70] The differences between the various studies lie primarily in the interpretation. The σ_H orientations are often at intermediate angles (40°–60°) to the SAF, not consistent with either the high-angle or the low-angle model, which understandably has confused the interpretation of these results. The only place where the high-angle, relatively weak fault model is clearly supported is along the creeping segment in central California.

[71] We perform two additional types of stress inversions in both northern and southern California. In one inversion we stack stress orientation versus distance profiles across all segments of the SAF to cancel out signals not related to the SAF. In the other we bin the seismicity using cluster analysis. Using high-quality focal mechanism data sets [*Hardebeck and Shearer*, 2002], we obtain intermediate angles near the SAF in both northern and southern California for both types of inversion.

[72] Alternatives to the strong-fault and relatively weak fault models are needed, which can explain the intermediate stress angles observed along much of the fault. One such model is an intermediate-strength SAF, with a coefficient of friction approximately half that of a strong fault or containing pore fluids at elevated pressure. Alternatively, observed stress rotations caused by earthquakes suggest low deviatoric stress magnitude at depth and variable stress orientation through the seismic cycle due to tectonic loading and seismic release. In this low-stress model all active faults must be weak, and the observed stress orientations along the SAF reflect its loading state and earthquake history, not its strength. Finally, the SAF may be a strong fault but not optimally oriented for failure.

[73] All of the viable models imply that the strength of the SAF is similar to the strength of other faults. In the strong-fault model all faults are equally strong, and in the weak-fault model all faults are equally weak. In the intermediate-strength model the major faults of the SAF system may have a strength as low as half that of minor faults. However, the SAF itself does not appear to be a particularly special fault. The relatively weak fault model, the only end-member model in which the SAF is significantly weaker than other faults, is ruled out by the stress orientation observations. Therefore characteristics of earthquake nucleation, rupture, triggering, and other behavior observed for other faults should be applicable to the SAF.

[74] **Acknowledgments.** We thank John Townend for providing us with his stress orientation model and Mark Zoback and Heidi Houston for helpful discussions. We thank Tom Hanks, David Oppenheimer, Delphine Fitzenz, Ann-Sophie Provost, and an anonymous reviewer for their thoughtful comments on the manuscript.

References

Andrews, D. J., and Y. Ben-Zion (1997), Wrinkle-like slip pulse on a fault between different materials, *J. Geophys. Res.*, *102*, 552–571.

Ben-Zion, Y., and P. E. Malin (1991), San Andreas Fault zone head waves near Parkfield, California, *Science*, *251*, 1592–1594.

Blanpied, M. L., D. A. Lockner, and J. D. Byerlee (1992), An earthquake mechanism based on rapid sealing of faults, *Nature*, *358*, 574–576.

Brudy, M., M. D. Zoback, K. Fuchs, F. Rummel, and J. Baumgärtner (1997), Estimation of the complete stress tensor to 8 km depth in the

KTB scientific drill holes: Implications for crustal strength, *J. Geophys. Res.*, *102*, 18,453–18,475.
Brune, J. N., T. L. Henyey, and R. F. Roy (1969), Heat flow, stress, and rate of slip along the San Andreas Fault, California, *J. Geophys. Res.*, *74*, 3821–3827.
Byerlee, J. (1978), Friction of rocks, *Pure Appl. Geophys.*, *116*, 615–626.
Byerlee, J. D. (1993), Model for episodic flow of high-pressure water in fault zones before earthquakes, *Geology*, *21*, 303–306.
Castillo, D. A., and S. H. Hickman (2000), Systematic near-field stress rotations adjacent to the Carrizo plain segment of the San Andreas Fault, in *Proceedings of the 3rd Conference on Tectonic Problems of the San Andreas Fault System*, edited by G. Bokelmann and R. L. Kovach, pp. 252–254, Stanford Univ. Press, Stanford, Calif.
Chéry, J., M. D. Zoback, and R. Hassani (2001), An integrated mechanical model of the San Andreas Fault in central and northern California, *J. Geophys. Res.*, *106*, 22,051–22,066.
Chester, F. M., J. P. Evans, and R. L. Biegel (1993), Internal structure and weakening mechanisms of the San Andreas Fault, *J. Geophys. Res.*, *98*, 771–786.
d'Alessio, M. A., A. E. Blythe, and R. Bürgmann (2003), No frictional heat along the San Gabriel fault, California: Evidence from fission-track thermochronology, *Geology*, *31*, 541–544.
Fitzenz, D. D., and S. A. Miller (2004), New insights on stress rotations from a forward regional model of the San Andreas Fault system near its Big Bend in southern California, *J. Geophys. Res.*, *109*, B08404, doi:10.1029/2003JB002890.
Hardebeck, J. L., and E. Hauksson (1999), Role of fluids in faulting inferred from stress field signatures, *Science*, *285*, 236–239.
Hardebeck, J. L., and E. Hauksson (2001), Crustal stress field in southern California and its implications for fault mechanics, *J. Geophys. Res.*, *106*, 21,859–21,882.
Hardebeck, J. L., and P. M. Shearer (2002), A new method for determining first-motion focal mechanisms, *Bull. Seismol. Soc. Am.*, *92*, 2264–2276.
Hauksson, E. (1994), State of stress from focal mechanisms before and after the 1992 Landers earthquake sequence, *Bull. Seismol. Soc. Am.*, *84*, 917–934.
Hauksson, E. (2000), Crustal structure and seismicity distribution adjacent to the Pacific and North America plate boundary in southern California, *J. Geophys. Res.*, *105*, 13,875–13,903.
Jennings, C. W. (1975), Fault map of California with locations of volcanoes, thermal springs, and thermal wells, *Calif. Geol. Data Map Ser. 1*, Calif. Div. of Mines and Geol., Sacramento.
Jones, L. M. (1988), Focal mechanisms and the state of stress on the San Andreas Fault in southern California, *J. Geophys. Res.*, *93*, 8869–8891.
King, G. C. P., R. S. Stein, and J. Lin (1994), Static stress changes and the triggering of earthquakes, *Bull. Seismol. Soc. Am.*, *84*, 935–953.
Lachenbruch, A. H., and J. H. Sass (1992), Heat flow from Cajon Pass, fault strength, and tectonic implications, *J. Geophys. Res.*, *97*, 4995–5015.
Lynch, J. C., and M. A. Richards (2001), Finite element models of stress orientation in well-developed strike-slip fault zones: Implications for the distribution of lower crustal strain, *J. Geophys. Res.*, *106*, 26,707–26,729.
Melosh, H. J. (1996), Dynamical weakening of faults by acoustic fluidization, *Nature*, *379*, 601–606.
Michael, A. J. (1984), Determination of stress from slip data: Faults and folds, *J. Geophys. Res.*, *89*, 11,517–11,526.
Michael, A. J. (1987), Use of focal mechanisms to determine stress: A control study, *J. Geophys. Res.*, *92*, 357–368.
Michael, A. J. (1991), Spatial variations in stress within the 1987 Whittier Narrows, California, aftershock sequence: New techniques and results, *J. Geophys. Res.*, *96*, 6303–6319.
Michael, A. J., and D. Eberhart-Phillips (2000), The Loma Prieta aftershocks: Heterogeneous stress or fault normal compression?, in *Proceedings of the 3rd Conference on Tectonic Problems of the San Andreas Fault System*, edited by G. Bokelmann and R. L. Kovach, pp. 237–251, Stanford Univ. Press, Stanford, Calif.
Michael, A. J., W. L. Ellsworth, and D. H. Oppenheimer (1990), Coseismic stress changes induced by the 1989 Loma Prieta, California earthquake, *Geophys. Res. Lett.*, *17*, 1441–1444.
Oppenheimer, D. H., P. A. Reasenberg, and R. W. Simpson (1988), Fault plane solutions for the 1984 Morgan Hill, California, earthquake sequence: Evidence for the state of stress on the Calaveras fault, *J. Geophys. Res.*, *93*, 9007–9026.
Provost, A.-S., and H. Houston (2001), Orientation of the stress field surrounding the creeping section of the San Andreas Fault: Evidence for a narrow mechanically weak fault zone, *J. Geophys. Res.*, *106*, 11,373–11,386.
Provost, A.-S., and H. Houston (2003), Stress orientations in northern and central California: Evidence for the evolution of frictional strength along the San Andreas plate boundary system, *J. Geophys. Res.*, *108*(B3), 2175, doi:10.1029/2001JB001123.
Reasenberg, P., and D. H. Oppenheimer (1985), FPFIT, FPPLOT and FPPAGE; Fortran computer programs for calculating and displaying earthquake fault-plane solutions, *U.S. Geol. Surv. Open File Rep., 85–0739*, 109 pp.
Rice, J. R. (1992), Fault stress states, pore pressure distributions, and the weakness of the San Andreas Fault, in *Fault Mechanics and Transport Properties of Rocks*, edited by B. Evans, and T.-F. Wong, pp. 475–503, Academic, San Diego, Calif.
Saffer, D. M., B. A. Bekins, and S. Hickman (2003), Topographically driven groundwater flow and the San Andreas heat flow paradox revisited, *J. Geophys. Res.*, *108*(B5), 2274, doi:10.1029/2002JB001849.
Scholz, C. H. (2000), Evidence for a strong San Andreas Fault, *Geology*, *28*, 163–166.
Scholz, C. H., and T. C. Hanks (2004), The Strength of the San Andreas Fault: A Discussion, in *Rheology and Deformation of the Lithosphere at Continental Margins*, edited by G. D. Karner et al., pp. 261–283, Columbia Univ. Press, New York.
Scholz, C. H., and F. J. Saucier (1993), What do the Cajon Pass stress measurements say about stress on the San Andreas Fault? Comment on "In situ stress measurements to 3.5 km depth in the Cajon Pass scientific research borehole: Implications for the mechanics of crustal faulting," by Mark D. Zoback and John H. Healy, *J. Geophys. Res.*, *98*, 17,867–17,870.
Sibson, R. H. (1992), Implications of fault-valve behaviour for rupture nucleation and recurrence, *Tectonophysics*, *211*, 283–293.
Sleep, N. H., and M. L. Blanpied (1992), Creep, compaction and the weak rheology of major faults, *Nature*, *359*, 687–692.
Spudich, P. A., M. G. Guatteri, K. Otsuki, and J. Minagawa (1998), Use of fault striations and dislocation models to infer tectonic shear stress during the 1995 Hyogo-ken Nanbu (Kobe) earthquake, *Bull. Seismol. Soc. Am.*, *88*, 413–427.
Townend, J., and M. D. Zoback (2000), How faulting keeps the crust strong, *Geology*, *28*, 399–402.
Townend, J., and M. D. Zoback (2001), Implications of earthquake focal mechanisms for the frictional strength of the San Andreas Fault system, in *The Nature and Tectonic Significance of Fault Zone Weakening*, edited by R. E. Holdsworth et al., *Geol. Soc. Spec. Publ.*, *186*, 13–21.
Townend, J., and M. D. Zoback (2004), Regional tectonic stress near the San Andreas Fault in central and southern California, *Geophys. Res. Lett.*, *31*, L15S11, doi:10.1029/2003GL018918.
Yin, Z. M., and G. C. Rogers (1995), Rotation of the principal stress directions due to earthquake faulting and its seismological implications, *Bull. Seismol. Soc. Am.*, *85*, 1513–1517.
Zoback, M. D. (2000), Strength of the San Andreas, *Nature*, *405*, 31–32.
Zoback, M. D., and G. C. Beroza (1993), Evidence for near-frictionless faulting in the 1989 (*M* 6.9) Loma Prieta, California, earthquake and its aftershocks, *Geology*, *21*, 181–185.
Zoback, M. D., and J. H. Healy (1992), In situ stress measurements to 3.5 km depth in the Cajon Pass scientific research borehole: Implications for the mechanics of crustal faulting, *J. Geophys. Res.*, *97*, 5039–5057.
Zoback, M. D., et al. (1987), New evidence on the state of stress of the San Andreas Fault system, *Science*, *238*, 1105–1111.

J. L. Hardebeck and A. J. Michael, U.S. Geological Survey, 345 Middlefield Road, MS 977, Menlo Park, CA 94025, USA. (jhardebeck@usgs.gov)